SF 298 MASTER COPY KEEP THIS COPY FOR REPRODUCTION PURPOSES

REPORT DOCUMENTATION PAGE

Form Approved
OMB NO. 0704-0188

1. AGENCY USE ONLY *(Leave blank)*	2. REPORT DATE	3. REPORT TYPE AND DATES COVERED
	20 Feb 97	Final

4. TITLE AND SUBTITLE
The Effect of Electromagnetic Fields on the Stability of Cylindrical Jets and Rods

5. FUNDING NUMBERS
DAAL03-92-K-0005

6. AUTHOR(S)
David L. Littlefield

7. PERFORMING ORGANIZATION NAMES(S) AND ADDRESS(ES)
Southwest Research Institute
PO Drawer 28510
San Antonio, TX 78228-0510

8. PERFORMING ORGANIZATION REPORT NUMBER

9. SPONSORING / MONITORING AGENCY NAME(S) AND ADDRESS(ES)
U.S. Army Research Office
P.O. Box 12211
Research Triangle Park, NC 27709-2211

10. SPONSORING / MONITORING AGENCY REPORT NUMBER
ARO 30539.10-EG

11. SUPPLEMENTARY NOTES
The views, opinions and/or findings contained in this report are those of the author(s) and should not be construed as an official Department of the Army position, policy or decision, unless so designated by other documentation.

12a. DISTRIBUTION / AVAILABILITY STATEMENT
Approved for public release; distribution unlimited.

12 b. DISTRIBUTION CODE

13. ABSTRACT *(Maximum 200 words)*

The effect of electromagnetic fields on the stability of cylindrical jets and rods was studied in this research. The goal of the program was to develop a better understanding of the disruptive mechanisms that electromagnetic fields might have on shape-charge jets and kinetic energy penetrators. A combined analytical and experimental approach was undertaken. Stability analyses were first performed on perfectly plastic, uniformly elongating jets when subjected to axial electric currents, and later extended to the case of elastic-plastic cylindrical rods. Results from the analyses were verified using a series of small scale, high voltage capacitive discharge experiments.

14. SUBJECT TERMS	15. NUMBER IF PAGES
Stability, Magnetohydrodynamics, Plasticity, Linear Perturbation Theory, Shape-Charge Jet, Kinetic Energy Projectile	**19**
	16. PRICE CODE

17. SECURITY CLASSIFICATION OR REPORT	18. SECURITY CLASSIFICATION OF THIS PAGE	19. SECURITY CLASSIFICATION OF ABSTRACT	20. LIMITATION OF ABSTRACT
UNCLASSIFIED	UNCLASSIFIED	UNCLASSIFIED	UL

TABLE OF CONTENTS

LIST OF FIGURES

1.0 STATEMENT OF PROBLEM

The effect of electromagnetic fields on the stability of cylindrical jets and rods was studied in this research. The goal of the program was to develop a better understanding of the disruptive mechanisms that electromagnetic fields might have on shape-charge jets and kinetic energy penetrators. A combined analytical and experimental approach was undertaken. Stability analyses were first performed on perfectly plastic, uniformly elongating jets when subjected to axial electric currents, and later extended to the case of elastic-plastic cylindrical rods. Results from the analyses were verified using a series of small scale, high voltage capacitive discharge experiments.

2.0 SUMMARY OF IMPORTANT RESULTS

2.1 Thermomechanical and Magnetohydrodynamic Stability of Cylindrical Stretching Jets

Stability calculations performed previously by Littlefield [4.1 - 4.6] showed that electromagnetic fields can alter the stability characteristics of isothermal, uniformly elongating plastic jets. The analyses demonstrated that axial electric currents always make the jet more unstable and increase the growth rate of naturally-occurring instabilities, even when small currents are employed. These results were then expanded to include high levels of electric current, where thermal energy transfer mechanisms become important [3.1, 3.2]. It was discovered that thermal softening of the jet due to Joule heating has a tendency to increase the growth rate of perturbations. This is illustrated in Figure 1, where a plot of the magnitude of perturbations to the radius of the jet are shown as a function of time for various initial wavelengths. Perturbations to the radius are normalized by their initial value, and time is normalized by the inverse of the axial strain rate. Values of dimensionless parameters Λ_{pp}, Ω, **E** and **R** were 100, 0.88, 0.0051, and 2.1, respectively. Physically Λ_{pp} represents a ratio of electromagnetic to inertial forces, Ω a ratio of inertial to plastic forces, **E** a ratio of kinetic energy to sensible heat and **R** a ratio of magnetic convection to diffusion. As is evident from the figure, the fastest growing disturbances have associated wavenumbers of about 2π, which corresponds to a wavelength equal to one half the jet diameter. A detailed description of the analysis and additional results can be found in refs. [3.1, 3.2, 3.4].

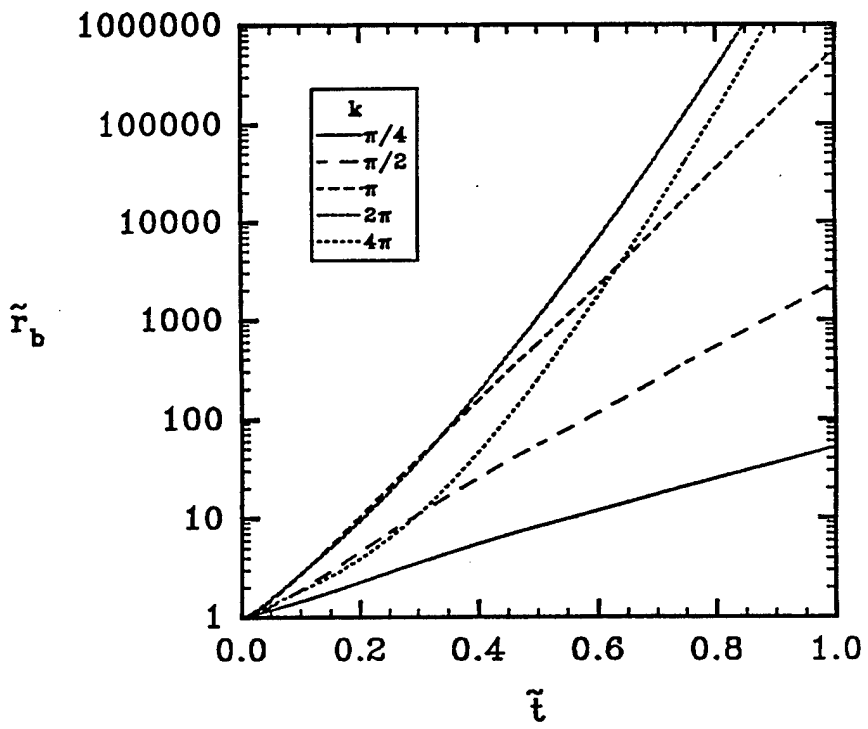

Figure 1. Normalized perturbed radius $\tilde{r}_b$ vs. normalized time $\tilde{t}$ at various wavenumbers for Λ_{pp} = 100, Ω = 0.88, E = 0.0051 and R = 2.1

2.2 Magnetomechanical Instabilities in Elastic-Plastic Cylinders

Constitutive models used in the stability analyses were then expanded from perfectly plastic behavior to the more general case of elastic-plastic flow. Results from the models indicated that stability of elastic-plastic rods is significantly altered when axial electric currents are introduced. In general, the frequency of oscillating perturbations is suppressed, and the growth rate of distending instabilities is hastened. Both of these tendencies appear to be intensified once plastic flow has initiated. This is illustrated in Figs. 2 and 3, where plots of the normalized frequency ω_i and normalized growth rate ω_r are shown, respectively, versus the normalized wavenumber k. The values of the parameters Φ and Ψ were 0.5 and 0, respectively. In Fig. 2, the parameter Λ_{ep} was set to 4, and in Fig. 3, growth rates for a range of values for Λ_{ep} is shown. Here the parameters Φ, Ψ, and Λ_{ep} physically represent a ratio of elastic to compression forces, a ratio of plastic to compression forces, and a ratio of electromagnetic to compression forces, respectively. The frequency spectrum shown in Fig. 2 exhibits substantial suppression when compared to the same result in the absence of electric current. Furthermore, the growth rates in Fig. 3 indicate that disturbances which grow in amplitude with time can occur, whereas in the absence of current distending perturbations are not possible; the growth rates of these disturbances and the wavenumber at which the maximum growth rate occurs tends to increase with the level of electric current. A complete description of these analyses and a more detailed discussion can be found in refs. [3.3, 3.5, 3.6], and for brevity will not be repeated here.

2.3 Computational and Experimental Studies of Magnetomechanical Instabilities in Cylindrical Metal Rods

The stability analyses of elastic-plastic rods was further continued to consider the effects of finite electrical conductivity, where it was also found that introduction of the current can cause both fluctuating and distending instabilities in the rod. A comparison of the results to similar calculations for perfectly conducting rods predicted that the effect of conductivity is to increase the growth rate is distending perturbations and lower the frequency of oscillatory disturbances. To validate the results from the theory, a series of experiments was performed by discharging electrical energy from a high voltage capacitor bank through thin copper rods. The development of axisymmetric distending instabilities in the rod was verified using a series of high speed, digital images. Comparisons with the model were reasonable and within the limitations of the analytical theory. These results have recently been reported in two conferences [3.7, 3.8], but have not yet been reported in the archival literature, and for convenience are presented here in more detail.

2.3.1 Introduction

The instability and breakup of cylindrical metal rods when subjected to large electromagnetic fields has become and area of increased interest over the past several years. An understanding of this phenomenon is critical to several industrial and military applications, including high voltage circuit interruption, electromagnetic forming, magnetically-confined fusion, and projectile disruption. For example, it is well known that when large electric currents are passed through cylindrical conductors that the cylinder has a tendency to *explode*, breaking up into a large number of thin, straited segments [4.7]. Although rapid expansion of the plasma formed from the vaporized wire certainly contributes to the observed breakup, electromagnetically-induced instabilities may also be partially responsible for the phenomenon. The same processes may also provide a means for effective protection of armored vehicles; for example, if a large electric current was introduced into a projectile, it might be disrupted in much the same way as an exploding wire. However, in order to utilize this technology effectively, a complete understanding of the coupling of electromagnetic effects to the mechanical behavior of the material must be obtained. In this paper, the theory governing the formation and propagation of fundamental magnetomechanical instability modes in metal cylinders is examined. The analysis is compared to results from small scale experiments performed using copper rods.

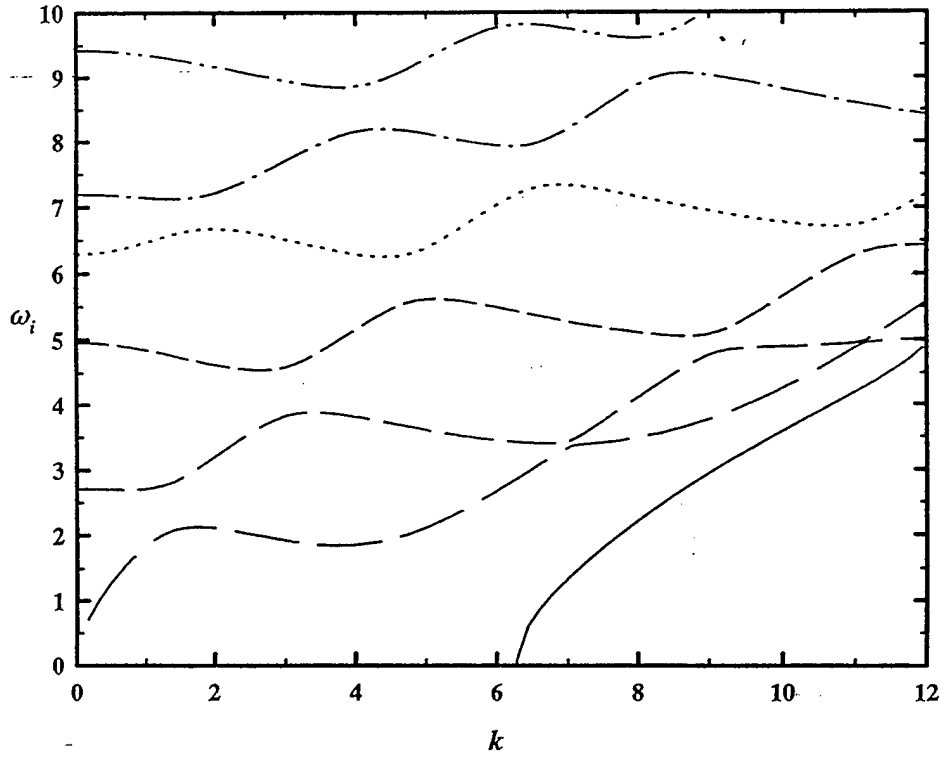

Figure 2. Normalized frequency ω_i vs. normalized wavenumber k for plastic disturbances in a cylinder with $\Phi = 1/2$, $\Psi = 0$ and $\Lambda = 4$.

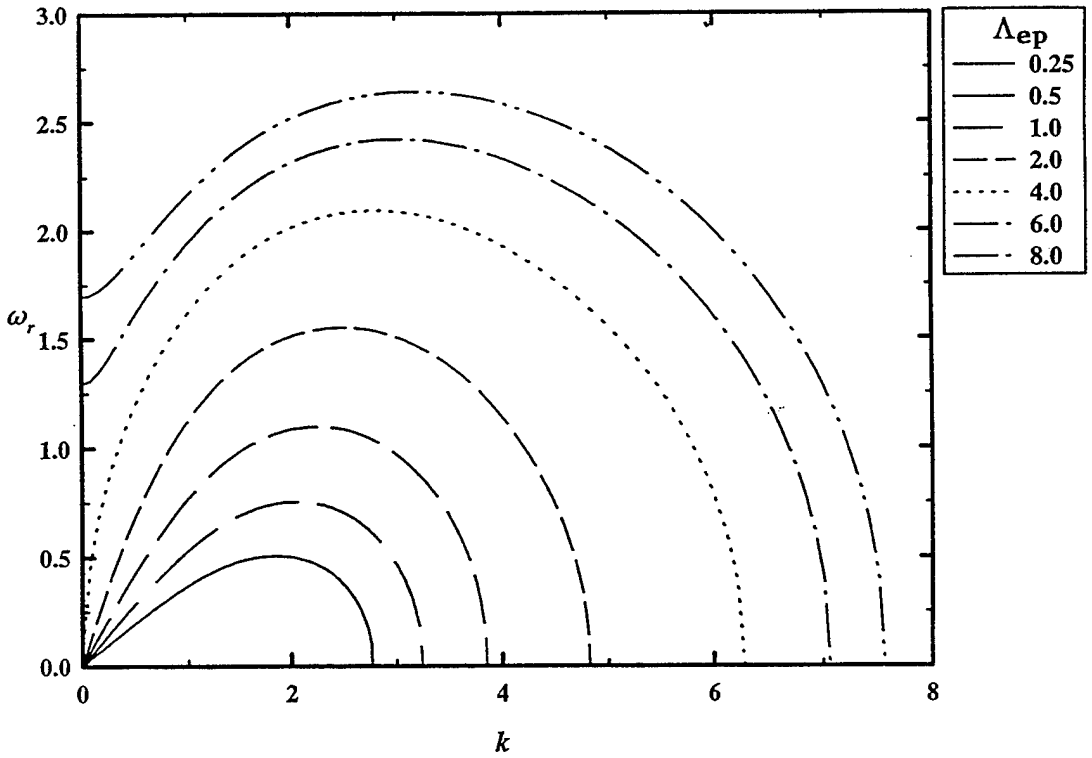

Figure 3. Normalized growth rate ω_r vs. normalized wavenumber k for plastic disturbances in a cylinder with $\Phi = 1/2$ and $\Psi = 0$.

In the analysis, the stability of an infinitely long, metal cylinder is considered. An axial electric current is introduced, creating an azimuthal magnetic field in the surrounding vacuum, and interacting with the current to generate an electromagnetic *pinching* force, directed towards the axis of the cylinder. The conductivity of the cylinder is assumed to be small enough so that the current remains completely diffused throughout the cross section; this condition is more realistic than the assumption of perfect conductivity made in previous analyses [3.3, 3.5, 3.6]. The electromagnetic force gives rise to a condition of uniform uniaxial strain in the cylinder. Two dimensional axi-symmetric perturbations to this motion are considered, and the equations governing the motion of these disturbances are derived using linear perturbation theory. These equations are solved to determine how the amplitude of small disturbances changes over time.

Results from a series of small scale experiments are presented to validate the theoretical predictions. Copper wires are subjected to an axial electric current caused by discharge from a bank of high voltage capacitors. Evolution of the instability and breakup of the cylinder is recorded through a series of high-speed, digital images.

2.3.2 Mathematical Model

Consider a long, cylindrical metal projectile that is deformed in its interior as a result of an applied electric current. The geometry of the cylinder is depicted in Fig. 4. The radius at an arbitrary point along the surface of the rod is denoted as $r_b(z,t)$, and the unit normal vector pointing into the surrounding vacuum is **n**. The equations governing axisymmetric motion in the interior of the projectile can be expressed as

$$\frac{\partial v_r}{\partial r}+\frac{v_r}{r}+\frac{\partial v_z}{\partial z}=-\frac{1}{K}\frac{\partial p}{\partial t}, \tag{1}$$

$$\rho\frac{\partial v_r}{\partial t}=-\frac{\partial p}{\partial r}+\frac{\partial \tau_{rr}}{\partial r}+\frac{2\tau_{rr}+\tau_{zz}}{r}+\frac{\partial \tau_{rz}}{\partial z}-\frac{B_\theta}{\mu}\left(\frac{\partial B_\theta}{\partial r}+\frac{B_\theta}{r}\right), \tag{2}$$

$$\rho\frac{\partial v_z}{\partial t}=-\frac{\partial p}{\partial z}+\frac{\partial \tau_{rz}}{\partial r}+\frac{\tau_{rz}}{r}+\frac{\partial \tau_{zz}}{\partial z}-\frac{B_\theta}{\mu}\frac{\partial B_\theta}{\partial z}, \tag{3}$$

and

$$\frac{\partial^2 B_\theta}{\partial r^2}+\frac{1}{r}\frac{\partial B_\theta}{\partial r}+\frac{\partial^2 B_\theta}{\partial z^2}=0, \tag{4}$$

where ρ is the density; K is the bulk modulus; μ is the magnetic permeability; v_r and v_z are the radial and axial components to the velocity, respectively; p is the pressure; τ_{ij} is a component of the deviatoric shear stress tensor; and B_θ is the azimuthal component of the magnetic field. Eq. (1) is the conservation of mass, Eqs. (2) and (3) the conservation of radial and axial momentum, respectively; and Eq. (4) the magnetic diffusion equation. When coupled with the appropriate constitutive relations in the cylinder, Eqs. (1) - (4) represent a complete system of equations to solve for the motion in the cylinder and in the surrounding vacuum.

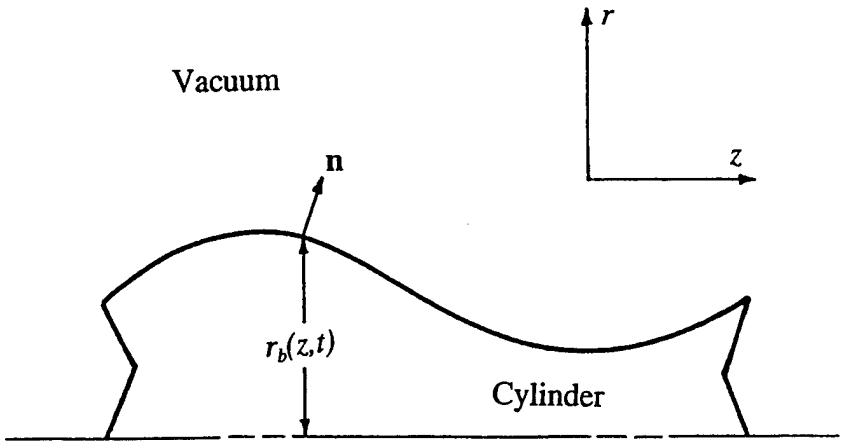

Figure 4. Model for Stability Calculations.

2.3.3 Idealized Motion

The governing equations given in the previous section admit a solution under uniaxial strain conditions. This idealized motion is characterized by a uniform radial compression of the rod as a result of the Lorentz force created by the applied electric current. Assuming the current is sufficient in magnitude to initiate yielding through the entire cross section of the cylinder, the pressure and radial displacement become

$$\tilde{p}_0 = \Lambda_{ep}(1-\tilde{r}^2) - \frac{\Psi\Phi}{3}; \quad \tilde{u}_{r0} = -\frac{\Lambda_{ep}\tilde{r}}{2}\left(1-\frac{\tilde{r}^2}{2}\right) + \frac{\Psi\Phi}{6}\tilde{r}, \tag{5}$$

where $\tilde{p} = p/K$, $\tilde{u}_r = u_r/r_{b0}$, $\Lambda_{ep} = \mu I^2/4\pi^2 r_{b0}^2 K$, $\Phi = G/K$, $\Psi = Y/G$, G is the shear modulus, Y is the yield strength, and the 0 subscript is used to imply a zeroeth-order solution. Here u_r is the radial displacement as is obtained from integrating the velocity with respect to time. The dimensionless parameters that appear in these solutions are Λ_{ep}, Φ, and Ψ, which physically represent a ratio of electromagnetic to compression forces, elastic shear to compression forces, and plastic to elastic shear; respectively.

2.3.4 Perturbation Equations

Solutions for the idealized motion in the rod given in the previous section are now subjected to a small disturbance. The equations governing the time evolution of these disturbances are derived by using linear perturbation theory. Solutions to these equations are used to identify perturbations that grow, decay or oscillate in amplitude with time.

The perturbation equations are formed in the usual way by expanding the independent variables in a power series of the form $f = f_0 + f_1\varepsilon + f_2\varepsilon^2 + \ldots$; where the 0, 1 and 2 subscripts denote zeroeth, first and second order approximations to the variable f, respectively; then retaining only terms which are of order ε. A natural consequence of this expansion is that the resulting linear differential equations can be Fourier analyzed with respect to time and the axial dimension, so that each of the Fourier modes depends on a normalized growth rate and ω and wavenumber k; that is

$$f_1 = \bar{f}(\bar{r})\exp(\omega\bar{t} + k\bar{z}), \tag{6}$$

where $\bar{t} = t/(r_{b0}\sqrt{\rho/K})$, $\bar{z} = z/r_{b0}$, $i = \sqrt{-1}$ and $\bar{f}$ is the amplitude of f_1. After the expansions are formed and the equations are solved, nontrivial solutions are found to exist only when a certain *dispersion relation* is satisfied; this relation describes the (ω, k) space where solutions exist to this eigenvalue problem. The details of the derivation and the resulting dispersion relation are described elsewhere [3.11], and for brevity will not be repeated here.

2.3.5 Solutions to Perturbation Equations

Solutions to the dispersion relations described in the previous section were generated for Φ = 1/2 and Ψ = 0.01, which are typical values for many metals. The dispersion relations also admit solutions for real and imaginary values for ω; imaginary values correspond to oscillatory instability modes and real values to distending modes. In the discussion that follows, ω_i is the imaginary component to ω and ω_r the real component, and are referred to as the normalized frequency and the normalized growth rate, respectively.

In Fig. 5, a plot of the stability spectrum for oscillatory modes is shown when Λ_{ep} = 1, where ω_i is shown as a function of the wavenumber k. The normalized frequency and wavenumber are related to the dimensional frequency f and wavelength λ_w as $f = \omega_i\sqrt{K/\rho}/2\pi r_{b0}$ and $\lambda_w = 2\pi r_{b0}/k$, respectively. Solutions are plotted along lines that exhibit similar deformation characteristics, and thus belong to the same deformation mode. There are many similarities between these results and the results shown elsewhere for elastic and elastic-plastic rods. For example, the frequency of perturbations tends to fluctuate with increasing wavenumber, as is seen in perfectly conducting elastic-plastic rods [3.6], but there is an overall tendency for the frequency to increase with k, as is observed in elastic rods [3.5, 3.9]. Suppression of the frequency occurs for the lowest oscillatory modes, as was observed for the perfectly conducting cylinder; however, the magnitude of the suppression is significantly larger. For example, when k = 10 the normalized frequency of the lowest mode shown in Fig. 5 is 1.105, whereas the frequency for a perfectly conducting rod under the same conditions is 3.961; and when no electric current is present this frequency becomes 4.041. The higher frequency modes are also influenced by the conductivity; albeit to a much lesser degree than the lowest mode. For example, when $k = \pi/2$ the normalized frequencies for the second mode are 2.000 and 2.132 in the present case and for perfect conductivity, respectively.

The introduction of electric current also produces distending instabilities in the rod. Shown in Fig. 6 is the normalized growth rate ω_r versus wavenumber for several different values of Λ_{ep}. The normalized growth rate is related to the dimensional growth rate α as $\alpha = \omega_r\sqrt{K/\rho}/r_{b0}$. It is evident from these results that the perturbations grow in amplitude at a faster rate as the current is increased. The fastest growing perturbation has a wavelength that tends to decrease with increasing electric current. Similar results are also observed in perfectly conducting rods [3.6]; however, for any given Λ_{ep} the magnitude of the growth rates are larger by a factor of two or more in the present case.

2.3.6 Experiments

In order to investigate the implications of the theory, a series of small scale experiments was performed. A 68 μF, 30 kV capacitor bank was used to discharge large electric currents through small copper rods. A schematic of the major components in the experimental setup are shown in Fig. 7. The capacitor bank is connected across a set of aluminum Walker plates [4.8] using a set of four RG-220 coaxial cables, and a 1.02 mm diameter, OFHC copper test cylinder was placed across these plates. In order to simplify the diagnostics, the tests were performed quasistatically and the rod remained stationary between the plates for the duration of the experiment. However,

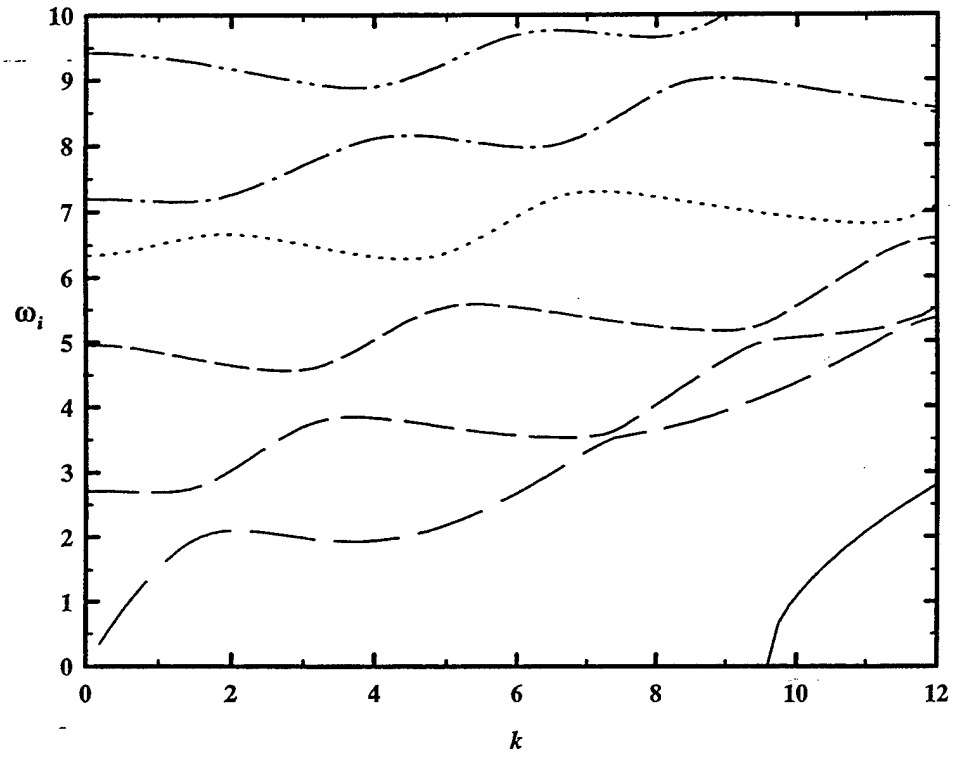

Figure 5. Normalized Frequency ω_i versus Normalized Wavenumber k for Perturbations in an Elastic-Plastic Cylinder with $\Phi = 1/2$, $\Psi = 0.01$ and $\Lambda_{ep} = 1$.

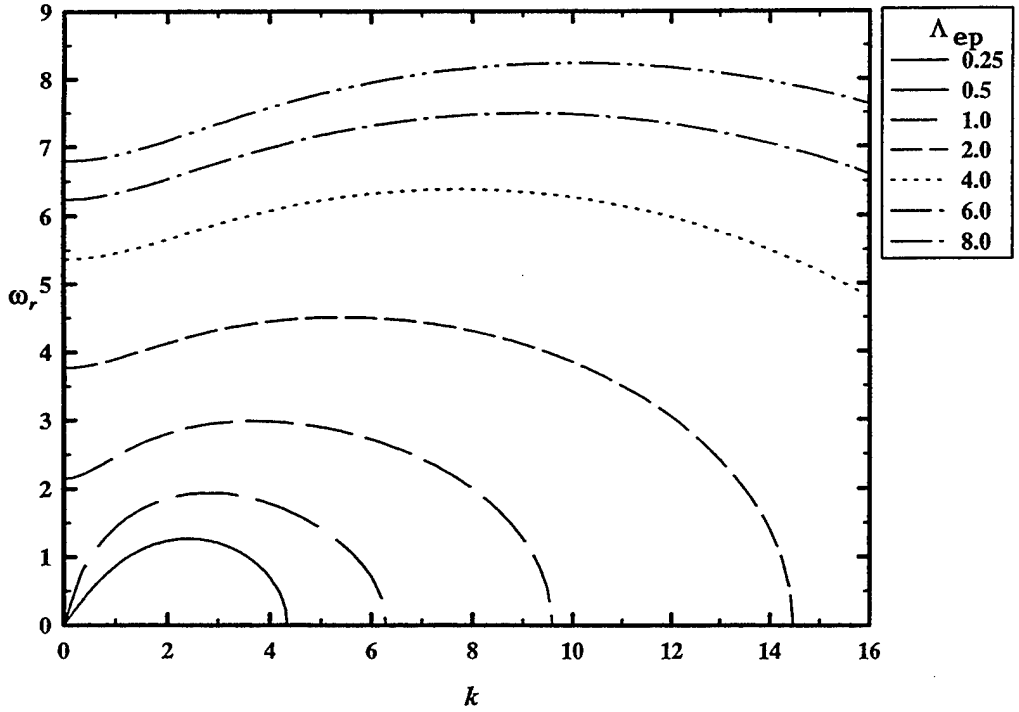

Figure 6. Normalized Growth Rate ω_r versus Normalized Wavenumber k for Perturbations in an Elastic-Plastic Cylinder with $\Phi = 1/2$ and $\Psi = 0.01$.

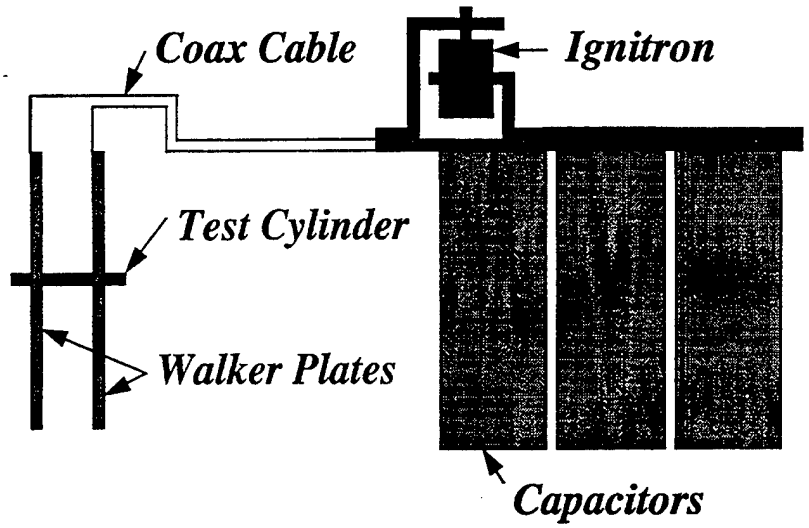

Figure 7. Schematic of Experimental Setup.

this does not eliminate the applicability of the results to moving projectiles, since the electromagnetic forces remain unchanged in a frame of reference moving along with the rod. The electric current was initiated using a 25 kV, 100 kA ignitron connected between the plates and ground.

Several forms of diagnostic measurements were used to interpret results from the experiments. High voltage dividers recorded the voltage across the capacitor bank and the Walker plates, and Pearson coils to measure the current flowing through the rod. B-dot probes were positioned radially around the circumference of the rod to measure the magnetic field. An Imacon 468 high speed, digital camera with a six-shot capability was used to image the experiment. The rod was illuminated by diffusing the beams from two 20 mW, He-Ne lasers, and a 632-nm bandpass filter was placed over the camera lens to filter out all wavelengths other than the light produced by the laser. This scheme helped eliminate much of the "flash" that typically occurs in high-voltage discharge experiments.

Voltage and current profiles produced from a typical low voltage experiment are shown in Fig. 8, where the current and voltage across the Walker plates is shown versus time for Test 39. The initial voltage across the plates is about 7.2 kV. Current and voltage profiles are representative of what is typically seen in the discharge of an RLC circuit. The peak current experienced by the rod is 42.4 kA, and occurs 17 μs after initiation. From the shape of the decay in the profile beyond 17 μs, the inductance and resistance of the test setup can be estimated. The inductance is about 850 nH, but the resistance tends to increase with time; at early times the resistance is about 28 mΩ, but later in the experiment the resistance increases to roughly 45 mΩ. A similar behavior was also observed when the experiment was repeated at higher voltages, but the time where the transition occurs in the resistance becomes progressively shorter.

Disruption of the rod is consistent with what is observed in the voltage and current profiles. Shown in Fig. 9 is an image from Test 39, showing the perturbation and breakup of the cylinder 58 μs after initiation of the current. Fig. 9 is a typical image showing the early stages of disruption for the cylinder at this particular voltage. Not only is the rod is beginning to break up into small segments, but it also shows indications of a *kink* instability developing, which tends to bend the rod out of plane. The wavelength of the segments is varied and falls within a range of roughly 1 to 2 times the radius of the rod, corresponding to wavenumbers of π and 2π,respectively. Arcing has occurred where a section of the rod has vaporized. Six microseconds later, the cylinder almost completely vaporizes, with indications of a vaporous halo surrounding remnants of the original rod.

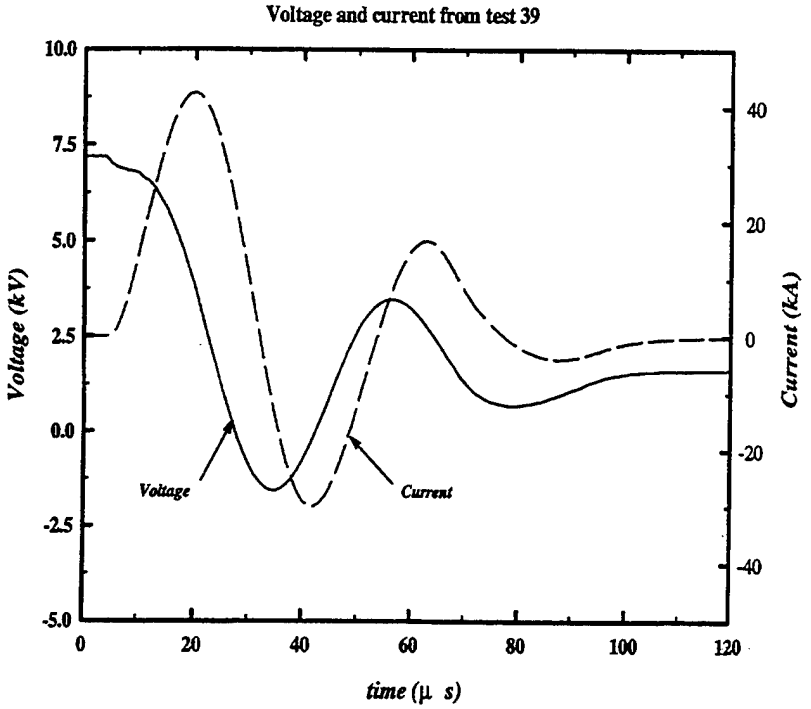

Figure 8. Voltage and Current Profiles from Test 39.

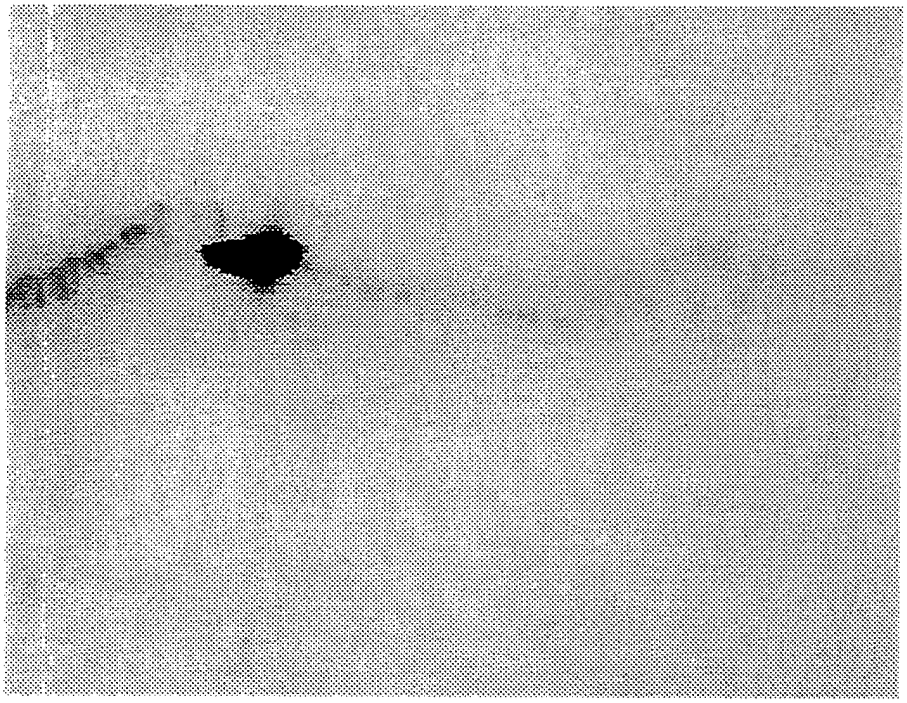

Figure 9. Digital Image (Displayed in Reverse Video for Clarity) Showing the Rod Disruption in Test 39, 58 μs After Current Initiation.

The change in resistance inferred from the current profiles also occurs at the same time the rod appears to be vaporizing; thus, it seems reasonable to assume that the increase is caused by the copper rod transitioning from a solid and/or liquid state and into a plasma.

When the current is increased, characteristics of the breakup of the cylinder change dramatically, and begin to look much like what is typically observed in exploding wire experiments [4.7]. Shown in Figs. 10 and 11 is a sequence of images from two different tests depicting the disruption in the rod, when a voltage of 13.9 kV is applied across the plates. Fig. 10 is from Test 47 at 13 μs; and Fig. 11 from Test 48 at 15 μs. During the early stages of disruption, the main effect of the current is to increase the diameter of the cylinder; after 11 μs, the diameter increased to 3.49 mm. By 13 μs, axisymmetric perturbations are beginning to develop in the interior of the rod, as shown in Fig. 10. The wavenumber associated with these perturbations is 0.427 based on the original radius of the cylinder, and 1.47 based on the radius at 11 μs. Fig. 11 indicates that these perturbations grow very rapidly in amplitude over the next two microseconds, which eventually disperse into a plasma cloud by 17 μs.

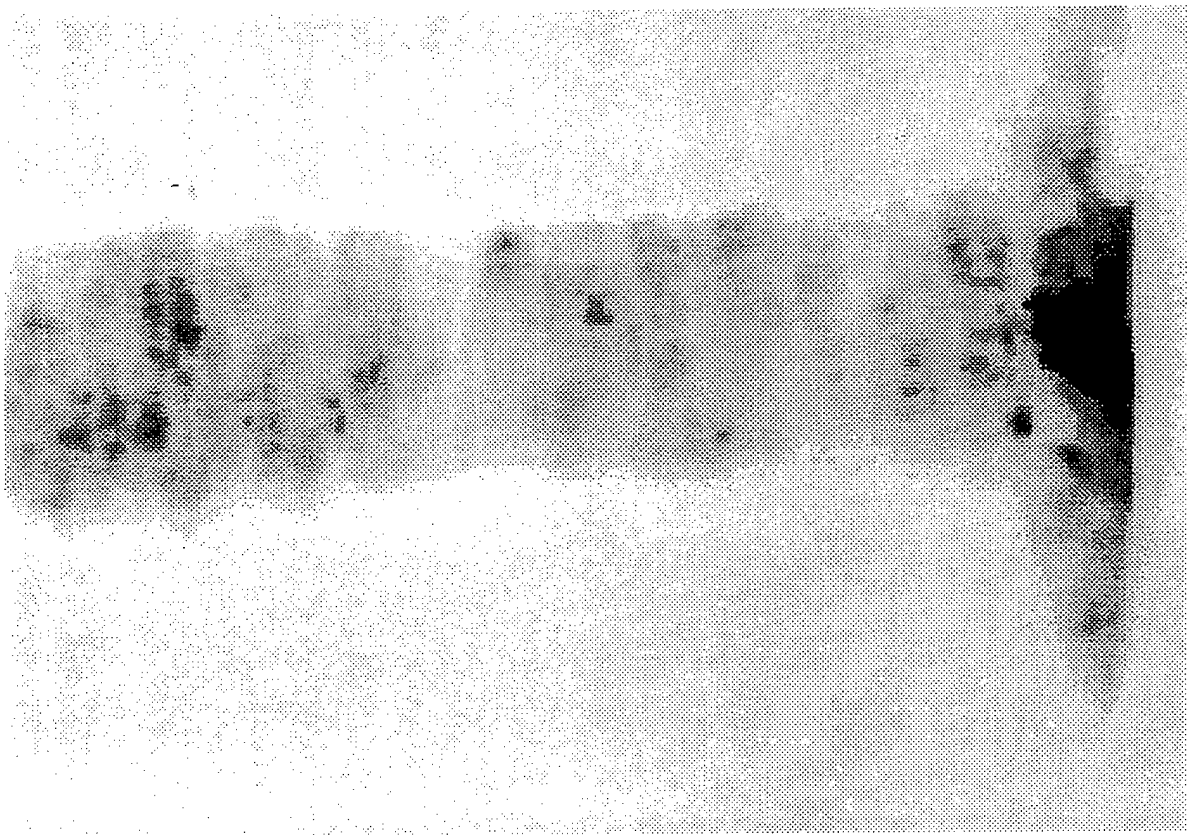

Figure 10. Digital image of the rod disruption from Test 47 at 13 μs (displayed in reverse video for clarity).

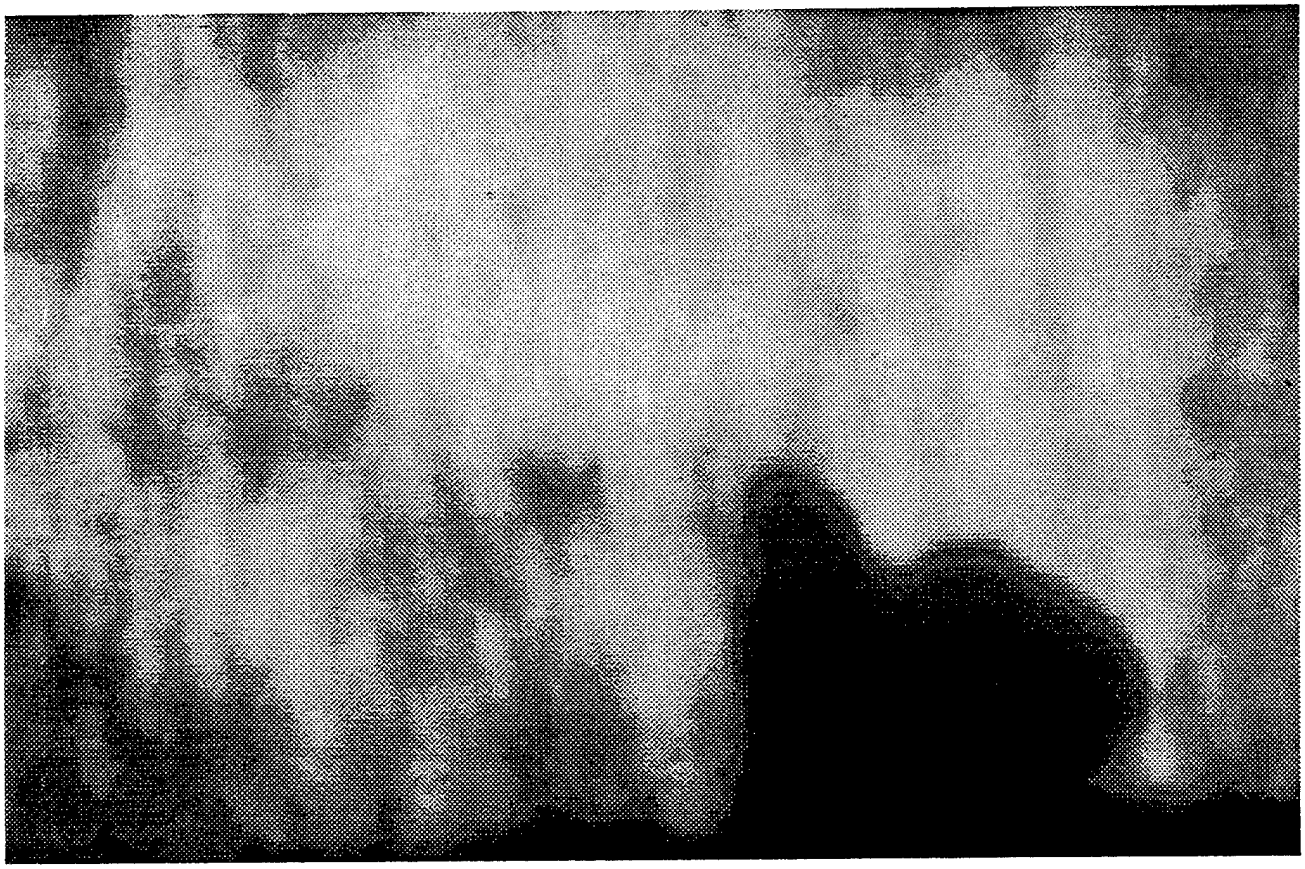

Figure 11. Digital image of the rod disruption from Test 48 at 15 μs. The Image is Partially Obscured by the Shadow of a B-dot Probe.

2.3.7 Comparisons Between Theory and Experiment

Results from the experiments can be used to make comparisons with the predictions from the perturbation theory. The analytical model assumes the rod is isothermal, so some adjustments to account for the temperature changes need to be applied. A simple calculation can be performed by integrating an energy equation of the form

$$\frac{\partial T}{\partial t} = \frac{\lambda}{\rho c_p}\left(\frac{I}{\pi r_b^2}\right)^2, \tag{7}$$

where T is the temperature, λ the resistivity, and c_p the specific heat. Using temperature-dependent values for λ and c_p, together with the current profiles from the experiments, the temperature can be determined. Assuming an initial temperature of 300K, the temperatures of the rod become 505K at 17 μs for the 13.9 kV experiment, and 710K at 60 μs for the 7.2 kV test, which are the approximate times in each experiment when disruption in the rod becomes the most prevalent. The temperature increase results in thermal softening of the rod, which can be accounted for in the model by making the appropriate adjustments in the yield strength. Using the corrected values together with the current profile from the experiments, eigenvalues that satisfy the dispersion relations governing the stability of the rod [3.10] can be determined. Applying the conditions from the higher voltage tests, these dispersion relations predict that maximum in ω_r occurs for $(\omega_r, k) = (0.1186, 1.277)$. This

wavenumber falls within the range of values measured from Tests 47 - 48. However, using the conditions from Test 39 the predicted maximum in ω_r occurs for $(\omega_r, k) = (0.0346, 0.8595)$. This wavenumber is not in agreement with the values seen in the experiment, where values of 3 to 6 were typically observed.

The predicted values for ω_r can also be compared with the growth rates in perturbations seen in the experiments. For example, the amplitudes of the disturbances shown in Figs. 7a - 7b can be measured directly and correspond to a growth rate of approximately 5.4×10^5 sec^{-1}. On the other hand, the growth rate corresponding to $\omega_r = 0.1186$ as predicted from the model is 8.7×10^5 sec^{-1}, which is reasonably close to the measured value. The growth rate from Test 39 could not be measured, but seemed to be quite small up until the point where the rod appeared to be vaporizing. The predicted value using the model is 2.5×10^5 sec^{-1}, which is large enough to be measured in a test; thus the model overpredicts the growth rate.

It seems likely that limitations of the theoretical model are responsible for disagreements between the experimental and analytical results. For example, in the model the rod is assumed to be solid and isothermal. Although the temperature changes predicted from the experiments seem low enough to validate this assumption, localization of the current from asymmetries or skin effects could cause "hot spots", resulting in localized melting and/or vaporization. Certainly the dynamics of the perturbation growth will change if this occurs. Furthermore, since the temperature prediction at breakup was higher for the 7.2 kV experiments, it seems likely that those tests might be more susceptible to localized phase changes; this may explain why inadequate agreement was obtained.

2.3.8 Conclusions

The stability of elastic-plastic cylinders has been considered in this analysis. In general, for a given level of electric current, isothermal conducting rods exhibit both distending and oscillatory perturbations. The growth rates of distending perturbations tend to be larger, and the frequency of oscillatory disturbances smaller, than is obtained for perfectly conducting rods. The formation of circulatory motion is also more aggressively suppressed when finite conductivity is taken into account.

Comparison of the analytical predictions with experimental results is reasonable, suggesting that instabilities developing while the rod is still a solid may be responsible for the observed breakup. The largest disagreements are obtained when temperature variations in the rod are expected to be the most important. Thus, a more detailed consideration of thermal effects is needed to improve the predictive capability of the model.

3.0 LIST OF PUBLICATIONS AND TECHNICAL REPORTS PUBLISHED

1. Littlefield, D. L., "Thermomechanical and Magnetohydrodynamic Stability in Shaped-Charge Jets," *Proceedings, 14th International Symposium on Ballistics,* **2**, pp. 155-164, 1993. *Nominated for the L. Zernow Award for best paper.*

2. Littlefield, D. L., "Thermomechanical and Magnetohydrodynamic Stability of Elongating Plastic Jets," *AIP Physics of Fluids,* **6**, pp. 2722-2729, 1994.

3. Littlefield, D. L., "The Disruption of Kinetic Energy Projectiles with Electromagnetic Fields", *Proceedings, 15th International Symposium on Ballistics*, **1**, pp. 275 - 282, 1995.

4. Powell, J. D., and Littlefield, D. L., "The Effect of Electromagnetic Fields on the Stability of Shaped Charge Jets in Walker Plate Experiments", *Proceedings, 3rd Ballistic Symposium on Classified and Controlled Topics*, Laurel, MD, November 14 - 15, 1995.

5. Littlefield, D. L., "Magnetomechanical Instabilities in Elastic-Plastic Cylinders, Part I: Elastic Response", *ASME Journal of Applied Mechanics*, **63**, pp. 734 - 741, 1996.

6. Littlefield, D. L., "Magnetomechanical Instabilities in Elastic-Plastic Cylinders, Part II: Plastic Response", *ASME Journal of Applied Mechanics*, **63**, pp. 742 - 749, 1996.

7. Littlefield, D. L., "Magnetomechanical Instabilities in Cylindrical Metal Rods", *Proceedings, 16th International Symposium on Ballistics,* **3**, pp. 269 - 278, 1996. *Awarded the Edith and Pei Chou Award for Best Paper by a Young Author.*

8. Littlefield, D. L., "Computational and Experimental Studies of Magnetomechanical Instabilities in Cylindrical Metal Rods", *Proceedings, 16th Army Symposium on Solid Mechanics*, Myrtle Beach, SC, October 16 - 18, 1996.

9. Littlefield, D. L., "The Effect of Finite Conductivity on Magnetomechanical Instabilities in Elastic-Plastic Cylinders, Part I: Elastic Response", submitted for publication in the *ASME Journal of Applied Mechanics.*

10. Littlefield, D. L., "The Effect of Finite Conductivity on Magnetomechanical Instabilities in Elastic-Plastic Cylinders, Part II: Plastic Response", submitted for publication in the *ASME Journal of Applied Mechanics.*

11. Littlefield, D. L., "The Effect of Finite Conductivity on Magnetomechanical Instabilities in Elastic-Plastic Cylinders, Part III: Low Strength Limit", submitted for publication in the *ASME Journal of Applied Mechanics.*

4.0 OTHER REFERENCES

1. Littlefield, D. L., and Powell, J. D., "The Effect of Electromagnetic Fields on the Stability of a Uniformly Elongating Plastic Jet," *AIP Physics of Fluids A*, **2**, pp. 2240-2248, 1990.

2. Powell, J. D. and Littlefield, D. L., "Effect of Electromagnetic Fields on the Stability of a Perfectly Conducting, Axisymmetric Shaped-Charge Jet", U. S. Army Ballistic Research Laboratory Technical Report BRL-TR-3108, June 1990.

3. Littlefield, D. L. and Powell, J. D., "The Effect of Electromagnetic Fields on the Stability of a Perfectly Conducting Shaped-Charge Jet," *Proceedings, 12th International Symposium on Ballistics*, **1**, pp. 359-368, 1990.

4. Littlefield, D. L., "Finite Conductivity Effects on the MHD Instabilities in Uniformly Elongating Plastic Jets," *AIP Physics of Fluids A*, **3**, pp. 1666-1673, 1991.

5. Littlefield, D. L., "Enhancement of Stability in Uniformly Elongating Jets with Electromagnetic Fields," *AIP Physics of Fluids A*, **3**, pp. 2927-2935, 1991.

6. Littlefield, D. L., "Enhancement of Shaped-Charge Jet Stability with Electromagnetic Fields," *"Proceedings, 13th International Symposiums on Ballistics,* **2**, pp. 393-400, 1992. *Nominated for the L. Zernow Award for best paper.*

7. Chace, W. G. and Moore, H. K. (ed), 1968, *Exploding Wires*, Plenum, New York.

8. Walker, E. H., 1973, U. S. Army Ballistic Research Laboratory Memorandum Report No. 2309.

5.0 LISTING OF SCIENTIFIC PERSONNEL SUPPORTED ON THE PROJECT

1. David L. Littlefield
2. Donald Grosch
3. Jerry Nixon
4. Ray Burgamy